Stub Column Tests on Stainless Steel Built-up Sections

H.X. Yuan[a],, Y.Q. Wang[a], Y.J. Shi[a], L. Gardner[b]*

[a]Key Laboratory of Civil Engineering Safety and Durability of China Education Ministry, Department of Civil Engineering, Tsinghua University, Beijing 100084, PR China

[b]Department of Civil and Environmental Engineering, Imperial College London, London SW7 2AZ, United Kingdom

Abstract

This paper presents twenty-eight stub columns tests on stainless steel built-up sections. The test specimens, including I-sections, square hollow sections (SHS) and rectangular hollow sections (RHS), were fabricated by shielded metal arc welding (SMAW) from hot-rolled plates of nominal thicknesses 6 mm and 10 mm. The twenty-eight stub columns, of two stainless steel alloys (austenitic EN 1.4301 and duplex EN 1.4462), were tested in pure axial compression. Both tensile and compressive material properties were obtained by means of coupon tests in three directions – longitudinal, diagonal and transverse to the rolling direction. Geometric imperfection measurements for each specimen were conducted by means of a calibrated electric guideway, and residual stress distributions in the built-up sections were determined by means of the sectioning method. The test strengths were used to evaluate the design strengths predicted by EN 1993-1-4 and the Continuous Strength Method (CSM). It was demonstrated that the predicted strengths from EN 1993-1-4 provisions were generally conservative, while the CSM predicted values were closer to the test strengths.

Keywords

Stainless steel; Stub column test; Local buckling; Residual stress; Built-up section

1 Introduction

The key advantage of stainless steel is its corrosion resistance, with durability often being a significant long term problem for ordinary carbon steel structures. As acceptance among engineers broadens, stainless steels are being increasingly used in a range of structural engineering applications [1-3].

In view of the material non-linearity and other disparities between stainless steel and carbon steel, the structural performance of stainless steel members has been investigated both experimentally and theoretically, with a focus on cold-formed sections. Stub column tests, aimed at studying the local buckling behaviour of cold-formed stainless steel sections, have been previously carried out by Rasmussen and Hancock [4], Young et al. [5-7], Gardner et al. [8-9], Kuwamura [10] and Zhen [11]. The tested stainless steels included both austenitic and duplex alloys, and the investigated various cross-section types included I-sections, square hollow sections (SHS), rectangular hollow sections (RHS), tubular sections with stiffeners [12], and oval hollow sections (OHS) [13]. However, far less experimental work has been carried out on stainless steel built-up sections, although these sections may be more suitable for meeting the strength requirements of the structural skeletons of buildings and bridges and may facilitate more economic structural design. For welded sections, Kuwamura [10] tested 16 H-shaped stub columns with 3 mm thick constitutive plates, Shen [14] reported tests on two grade EN 1.4301 welded I-section stub columns and Saliba and Gardner [15] carried out experiments on lean duplex stainless steel welded I-sections. Clearly, more experimental work on stainless steel built-up sections involving multiple section types and alloys are required.

Traditionally, cross-section compression resistance is calculated, following section classification, as either the yield load for stocky sections or a reduced capacity to account for local buckling occurring prior to yielding for slender sections. The reduced capacity may be determined using the effective width method, as employed in EN 1993-1-4. As an alternative approach to the classical cross-section classification and effective width concepts, the newly developed Continuous Strength Method (CSM) is a strain based design method that allows for the exploitation of strain hardening in the case of stocky cross-sections [16]. The underlying concept of the CSM makes it well suited to the design of structures of non-linear metallic materials, which exhibit no distinct yield point [17].

This paper presents a comprehensive experimental programme on stainless steel stub columns with built-up sections, including the measurement of initial geometric imperfections, determination of residual stresses and full-scale loading tests. The test strengths are used to assess the existing design provisions of EN 1993-1-4 and the newly developed CSM. Furthermore, the conducted experimental research could remedy the lack of test data available on the stainless steel built-up sections. It could also directly contribute to the establishment of the first Chinese design standard for structural stainless steel, development of which is currently underway

Paper Presented by Huanxin Yuan - yuanhx09@gmail.com

2 Material Properties from Tensile and Compressive Coupon Tests

Two different stainless steel alloys, namely austenitic grade EN 1.4301 and duplex grade EN 1.4462, were considered in the study. According to the ASTM A959 designation system [18], these two alloys are equivalent to type 304 and 2205, respectively. For the EN 1.4301 material, the accurately measured thicknesses of the hot-rolled coil plates were 6.00 mm and 10.00 mm, while the corresponding measured values of the EN 1.4462 hot-rolled coil plates were 6.00 mm and 10.20 mm. All material of the same alloy and thickness came from the same batch, and had quality certificates for basic chemical compositions and mechanical properties.

The tensile and compressive coupons were cut directly from the original plates. The coupon dimensions and testing procedure conformed to both the Chinese testing standards and the ASTM test methods [19-22]. The layout of coupons, cut in the longitudinal (plate rolling direction), diagonal and transverse directions, is shown in Fig. 1. There were a total of 72 tensile and compressive coupons, since each stainless steel alloy had two different thicknesses and three repeated coupons were tested for each case. The coupons were all tested using a 100 kN capacity universal testing machine. An extensometer and two orthogonal strain gauges were adopted in the tensile tests; while for the compressive coupons, the compressive strains were simply measured using two unidirectional strain gauges. The compressive coupon tests were performed by means of a special bracing jig to prevent premature minor axis buckling, yet allow transverse expansion. The jig employed in this study, which is similar to a previously used devise [8], is shown in Fig. 2.

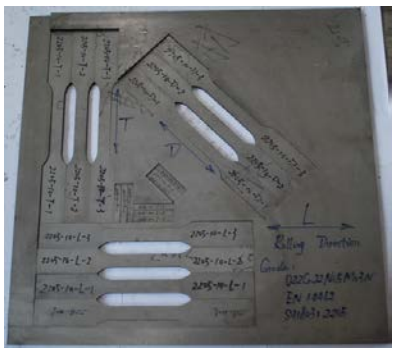

Fig. 1. Layout of tensile and compressive coupons

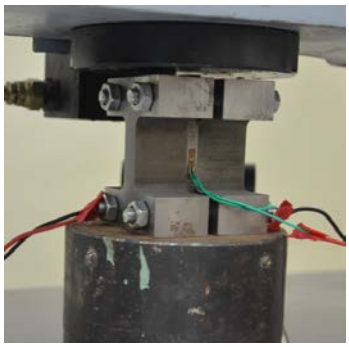

Fig. 2. Compressive bracing jig

Average measured tensile and compressive material properties from the test coupons are summarized in Tables 1 and 2, respectively, where the following symbols are used: E_0 is the Young's modulus, v is the Poisson's ratio, acquired from the ratio of the measurements from two orthogonal strain gauges, $\sigma_{0.01}$, $\sigma_{0.2}$ and $\sigma_{1.0}$ are the 0.01%, 0.2% and 1% proof stresses, respectively, σ_u is the ultimate tensile stress, ε_u is the strain at the ultimate tensile stress (not obtained for all coupons due to the limited range of the extensometer), ε_f is the plastic strain at fracture, measured from the fractured tensile coupons as elongation over the standard gauge length, and n is the Ramberg-Osgood strain hardening coefficient. The 1.0% proof stress $\sigma_{1.0}$ was provided for use in the compound Ramberg-Osgood model [17]. The ratios of 0.2% proof strengths given in the final column of Tables 1 and 2 provide a measure of the anisotropic characteristics of the materials. The asymmetry between tension and compression properties of the two stainless steel alloys can also be observed from the test results. Two sets of stress-strain curves are plotted in Fig. 3, revealing typical non-linear characteristics and illustrating the degree of anisotropy.

Table 1 Average measured material properties from tensile coupon tests

Grade	t (mm)	Direction	E_0 (MPa)	v	$\sigma_{0.01}$ (MPa)	$\sigma_{0.2}$ (MPa)	$\sigma_{1.0}$ (MPa)	σ_u (MPa)	ε_u (%)	ε_f (%)	n	Anisotropic ratio (DT/LT or TT/LT)
1.4301	6.00	LT	188600	0.251	186.3	312.6	354.4	695.7	-	60.6	5.8	-
		DT	194000	0.272	227.9	310.9	352.0	678.6	-	62.5	9.6	0.99
		TT	201900	0.300	241.3	318.7	364.5	683.5	-	59.2	10.8	1.02
1.4301	10.00	LT	188800	0.272	213.0	328.5	379.4	659.8	-	55.5	6.9	-
		DT	197200	0.281	239.6	354.4	401.4	671.2	-	56.7	7.7	1.08
		TT	199100	0.287	248.4	356.9	403.0	673.0	-	54.9	8.3	1.09
1.4462	6.00	LT	193200	0.204	404.4	605.6	665.0	797.9	21.0	34.6	7.4	-
		DT	191000	0.285	451.2	635.3	695.9	803.3	19.8	38.2	8.8	1.05
		TT	221200	0.244	470.2	696.4	767.0	869.0	17.1	31.2	7.6	1.15
1.4462	10.20	LT	191200	0.205	366.8	574.8	651.2	775.0	20.6	35.4	6.7	-
		DT	186200	0.280	409.4	604.1	663.1	763.7	21.1	36.1	7.7	1.05
		TT	222400	0.233	460.9	681.5	732.7	838.0	16.7	30.7	7.7	1.19

LT: Longitudinal Tension, DT: Diagonal Tension, TT: Transverse Tension.

Table 2 Average measured material properties from compressive coupon tests

Grade	t (mm)	Direction	E_0 (MPa)	$\sigma_{0.01}$ (MPa)	$\sigma_{0.2}$ (MPa)	$\sigma_{1.0}$ (MPa)	n	Anisotropic ratio (DC/LC or TC/LC)
1.4301	6	LC	182300	177.2	281.5	347.3	6.5	-
		DC	205600	217.7	311.3	366.3	8.4	1.11
		TC	219400	232.0	324.4	383.8	8.9	1.15
1.4301	10	LC	198700	195.1	320.5	393.0	6.0	1.00
		DC	205700	235.6	348.0	408.8	7.7	1.09
		TC	210800	267.3	363.8	421.1	9.7	1.13
1.4462	6	LC	191900	360.6	553.0	667.4	7.0	-
		DC	193500	457.3	625.6	704.0	9.6	1.13
		TC	226900	432.4	666.1	764.9	6.9	1.20
1.4462	10.2	LC	190400	342.5	546.9	644.0	6.4	-
		DC	193600	415.0	604.5	685.2	8.0	1.11
		TC	226600	432.5	644.5	738.3	7.5	1.18

LC: Longitudinal Compression, DC: Diagonal Compression, TC: Transverse Compression.

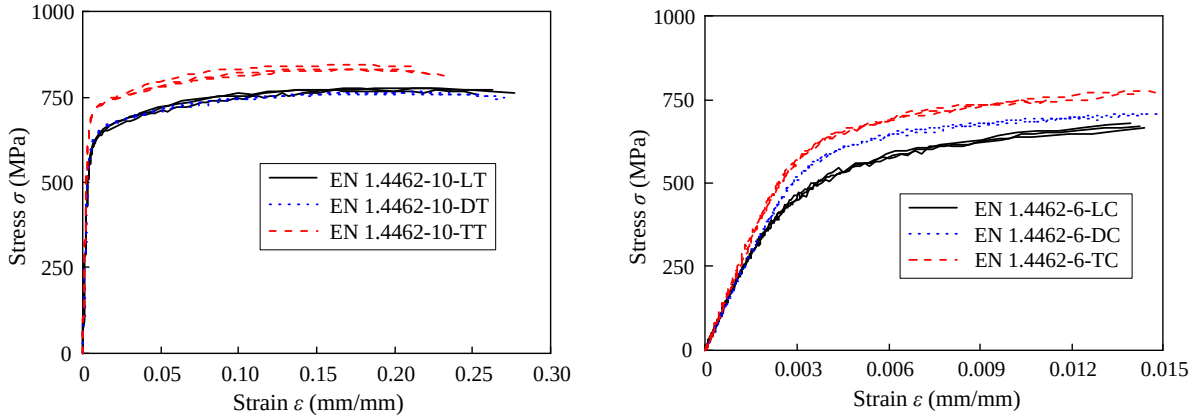

(a) Tension (b) Compression

Fig. 3 Stress-strain curves of the tested coupons

3 Fabrication of stub column specimens

The test programme comprised a total of 28 stub column tests on specimens with built-up sections. The constitutive plates of the specimens were cut from hot-rolled coil by water jet cutting. Zero heat input was thus induced into the plates, eliminating the risk of distortion during the cutting process. All constitutive plates of stub column specimens were cut parallel to the plate rolling direction.

Shielded metal arc welding (SMAW), also known as manual metal arc welding (MMA), was used to fabricate the built-up sections. Welding rods were selected to match the parent material [23], with type E308 corresponding to the EN 1.4301 material and type E2209 corresponding to the EN 1.4462 material. Fillet and butt welds were adopted to build up the I-section and hollow section specimens respectively, as show in Fig. 4. A weld size of 5 mm was selected for the two kinds of welds with both strength and construction requirements taken into consideration. Significant welding distortion was observed during fabrication, due to the high coefficients of thermal expansion and low thermal conductivities of the materials. The residual deformation of the I-section flanges, in particular, required special attention. Two techniques, namely reverse bending of the I-section flange plates before assembling and symmetric welding sequences, were introduced to alleviate the welding distortions. Subsequent to welding, additional straightening of the specimens by means of a hydraulic press with special clamping apparatus was implemented.

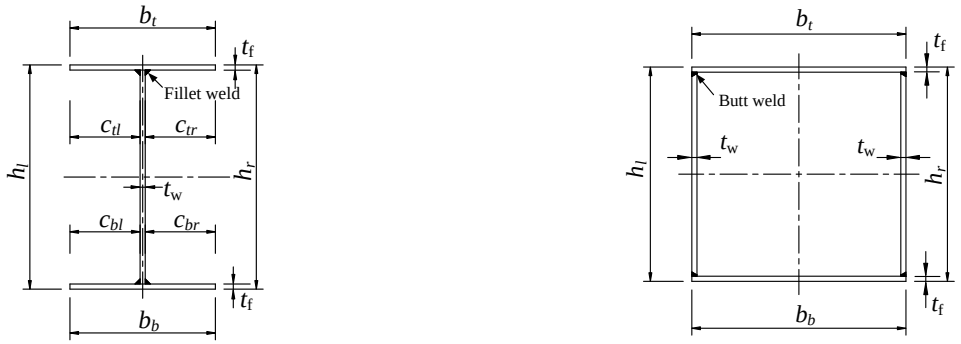

(a) I-section (b) SHS or RHS

Fig. 4 Definition of symbols and weld locations

The stub column specimens were designed to cover a wide range of plate width-to-thickness ratios, including both internal and outstand plate elements. In order to eliminate end effects yet prevent overall buckling, the lengths of the stub columns specimens lay within the limits set by the Structural Stability Research Council [24], at a nominal value of three times the depth of the section. In some cases, the lengths were rounded to convenient values for manufacturing. Flatness demands of the column end planes were achieved by a wire-cutting technique. Three types of sections (I-section, SHS and RHS) were considered in the programme, with the definition of symbols and weld locations graphically illustrated in Fig. 4. Geometric dimensions of the test specimens were measured at three different cross-sections – the mid-length section and two sections at 50 mm from the specimen ends. The average measured dimensions for the 28 stub column specimens are presented in Tables 3 and 4. The specimen labelling convention indicates the section type, the material grade and the nominal section depth. Specimen I304-192-a, for example, is an I-section, of grade EN 1.4301 (304) alloy and 192 mm nominal section depth. The last symbol 'a' was used to distinguish between the specimens with the same section depth.

Table 3 Average measured geometric dimensions for I-section specimens

Specimen	b_t	b_b	h_l	h_r	t_w	t_f	c_{tl}	c_{tr}	c_{bl}	c_{br}	L	A(mm^2)
I304-150	149.5	149.5	150.1	149.0	6.00	10.00	70.3	73.2	71.3	72.2	449.6	3767.2
I304-192	185.2	185.3	193.0	194.7	6.00	6.00	90.5	88.7	90.5	88.8	598.0	3314.1
I304-192-a	126.4	126.1	193.1	195.3	6.00	6.00	60.5	59.9	60.0	60.1	601.1	2608.4
I304-252	246.1	245.3	252.7	253.8	6.00	6.00	120.5	119.6	119.6	119.6	779.9	4395.9
I304-260	165.4	166.0	258.9	259.0	6.00	10.00	79.7	79.7	80.2	79.8	779.9	4747.6
I304-282	185.7	185.5	282.6	283.2	6.00	6.00	89.2	90.5	89.6	89.9	850.4	3852.9
I304-312	305.5	305.5	314.3	313.1	6.00	6.00	148.4	151.1	148.8	150.7	951.6	5476.3
I304-320	205.7	205.5	319.7	319.5	6.00	10.00	99.8	99.9	100.0	99.6	961.6	5909.8
I304-372	246.1	246.0	373.9	372.7	6.00	6.00	120.6	119.5	119.9	120.1	1117.8	5120.3
I304-462	185.8	186.2	462.9	462.2	6.00	6.00	90.5	89.3	89.9	90.3	1400.7	4935.0
I2205-150	149.0	151.0	150.1	151.2	6.00	10.20	70.3	72.7	72.4	72.6	449.4	3841.6
I2205-192-a	126.2	125.4	194.0	192.2	6.00	6.00	60.0	60.2	59.3	60.1	600.0	2596.3
I2205-200	124.8	125.0	201.1	200.0	6.00	10.20	58.7	60.1	58.5	60.5	601.4	3581.7
I2205-252	245.0	245.5	254.5	251.2	6.00	6.00	118.9	120.1	119.2	120.3	780.0	4388.3
I2205-372	245.0	245.0	373.0	372.7	6.00	6.00	119.0	120.0	118.8	120.2	1117.0	5105.2

All dimensions except the area A are in mm.

Table 4 Average measured geometric dimensions for RHS and SHS specimens

Specimen	b_t	b_b	h_l	h_r	t_w	t_f	L	A(mm^2)
R304-200	100.4	100.4	199.7	200.1	6.00	6.00	600.1	3459.2
R304-300	200.2	199.9	299.6	299.8	6.00	6.00	901.2	5852.8
R304-400	200.5	199.5	400.5	400.0	6.00	6.00	1201.5	7059.0
S304-130	130.1	130.4	129.5	130.0	6.00	6.00	399.7	2975.8
S304-200	200.5	200.0	200.5	200.5	6.00	6.00	600.4	4665.0
S304-300	301.1	301.5	301.3	300.0	6.00	6.00	900.9	7079.2
S304-350	350.0	351.0	350.1	350.1	6.00	6.00	1051.0	8262.8
R2205-200	100.0	100.8	200.2	200.0	6.00	6.00	601.0	3462.2
R2205-300	201.0	200.8	301.1	300.0	6.00	6.00	900.1	5873.6
R2205-400	200.5	199.8	401.4	401.1	6.00	6.00	1201.2	7072.6
S2205-130	130.5	130.5	130.4	130.2	6.00	6.00	399.5	2985.8
S2205-300	300.2	299.5	301.3	300.7	6.00	6.00	898.9	7065.7

S2205-350	349.7	349.8	350.4	350.3	6.00	6.00	1051.0	8256.8

All dimensions except the area A are in mm.

4 Initial geometric imperfections and residual stresses

4.1 Measurement of initial geometric imperfections

Although the distortions of the test specimens were minimised, as described in the previous section, initial geometric imperfections still exist. Schematic profiles of typical local geometric imperfection distributions measured in the I-sections and SHS/RHS are plotted in Fig. 5. The local imperfection magnitude w_0 of a cross-section was defined in relation to the junctions between flanges and webs.

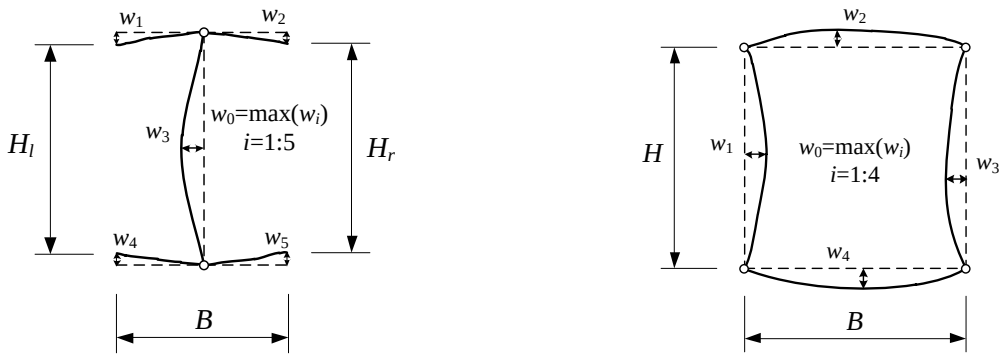

Fig. 5 Schematic view of local geometric imperfections

A special tool was devised for the continuous measurement of initial geometric imperfections in the test specimens. Combined with a digital linearly-varying displacement transducer (LVDT), a calibrated electric guideway was introduced to accomplish the measuring procedure, as shown in Fig. 6. The helical guideway would move the LVDT at a constant rate along a specified path by means of a magnetic stepping motor. In this study a uniform translational speed of 2 mm/s was used to achieve a balance between accuracy and measuring efficiency. The recorded positional data and corresponding time points were used to derive a continuous imperfection distribution and hence acquire the local imperfection amplitude. The initial local imperfections at three representative cross-sections were measured for each test specimen. The locations of the measured cross-sections, which were at the mid-length section B and two sections 50 mm from the specimen ends (sections A and C), referred to in [25], are shown in Fig. 7.

Fig. 6 Measurement of local geometric imperfections

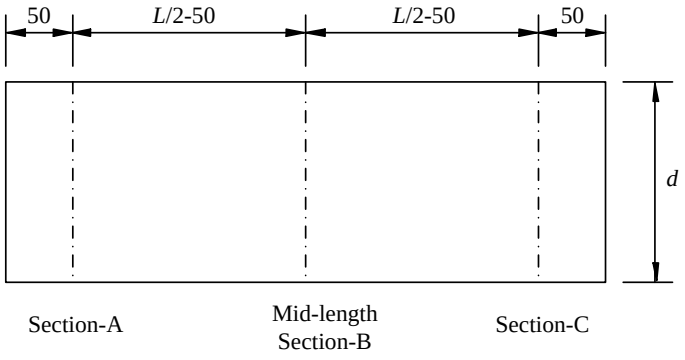

Fig. 7. Location of measured cross-sections

The measured local imperfection distributions for two typical stub column specimens, Specimens I304-462 and S2205-350, are presented in Fig. 8. All the imperfection details such as distribution, magnitude and convex direction were extracted from the distribution curves. With the aim of simplification and convenience, the imperfection magnitude for each specimen was determined as the maximum value among the three cross-sections. In accordance with the described method, the local imperfection magnitudes for all stub column specimens are reported in Table 5.

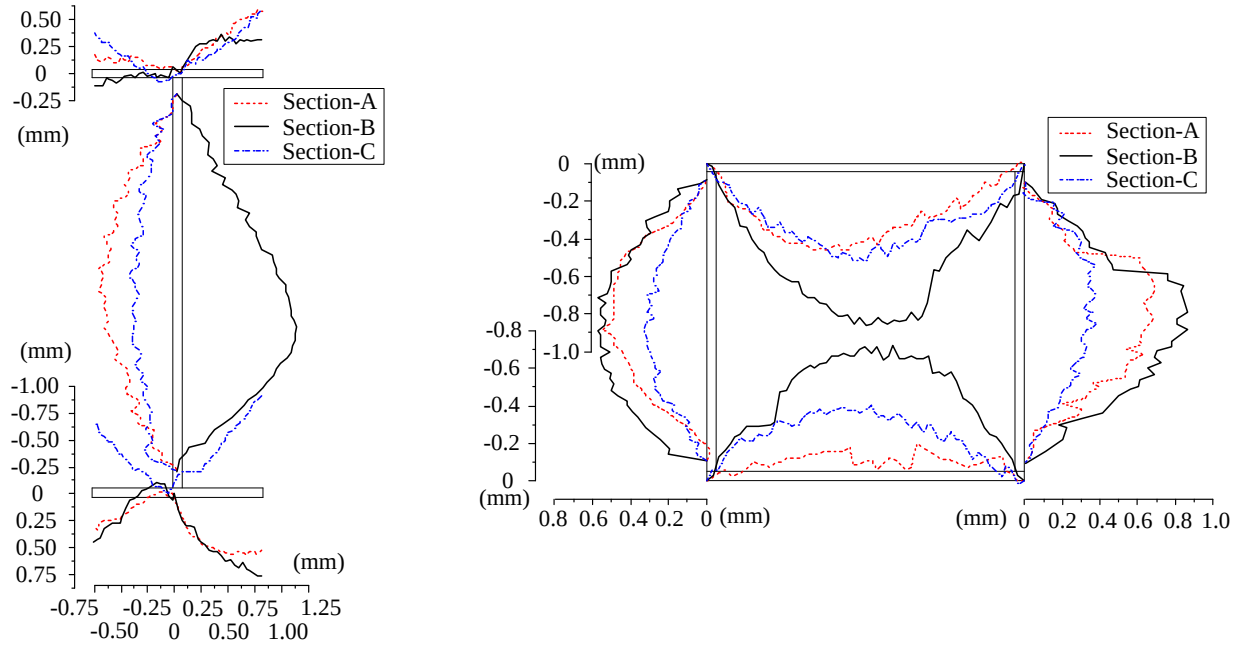

(a) I304-462 (b) S2205-350

Fig. 8 Measured local imperfection distributions for the Specimens I304-462 and S2205-350

Table 5 Measured initial local geometric imperfection amplitudes for the test specimens

Specimen	Amplitude w_0 (mm)	Specimen	Amplitude w_0 (mm)
I304-150	0.55	R304-200	0.23
I304-192	1.05	R304-300	0.46
I304-192-a	0.79	R304-400	0.42
I304-252	1.17	S304-130	0.21
I304-260	0.67	S304-200	0.66
I304-282	0.87	S304-300	0.59
I304-312	1.51	S304-350	0.72
I304-320	0.71	R2205-200	0.51
I304-372	1.20	R2205-300	0.49
I304-462	1.11	R2205-400	1.38
I2205-150	0.59	S2205-130	0.18
I2205-192-a	0.60	S2205-300	0.52
I2205-200	0.71	S2205-350	0.86
I2205-252	0.55		
I2205-372	0.77		

4.2 Determination of residual stresses

Residual stresses induced by the welding procedure were determined by means of the classical sectioning method [26]. This method has been successfully used for decades and has proven to be an adequate, accurate and economical measuring technique. The test pieces were prepared along with the stub column specimens, and cut from the same member length, as shown in Fig. 9. The central portion was extracted by a wire-cutting technique from the original stock to determine the residual stresses, while one of the remaining portions was used as the stub column specimen. Following this approach, the obtained residual stress distribution would closely match that of the corresponding stub column.

The complete sectioning was performed on an automated electric spark wire-cutting machine that brought about no extra heat input, as shown in Fig. 10. The width of each strip was set as 10 mm with small discrepancies. A standard Whittemore gauge with a gauge length of 254 mm (10 in.), was used to take initial and final readings (prior to and subsequent to sectioning) from pairs of gauge holes. Accurate measurements were achieved by ensuring the perpendicular location of the gauge, making any temperature correction from the reference bar and taking three repeated sets of readings for each strip.

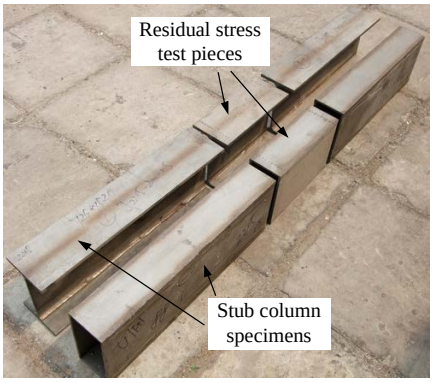

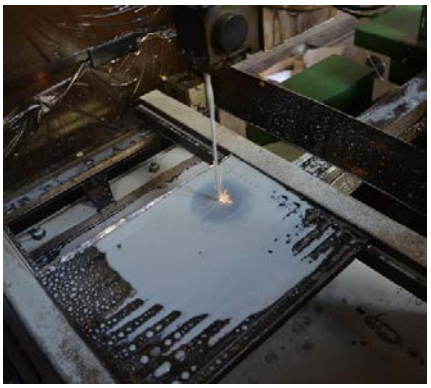

Fig. 9 Arrangement of the residual stress test pieces **Fig. 10 Electric spark wire-cutting process**

The relaxed stresses could be computed directly by multiplying the released strain by the measured Young's modulus. In view of the asymmetry in tension and compression of the stainless steel alloys, tensile and compressive properties were used separately to calculate the corresponding residual stresses. The measured magnitude and distribution of residual stresses from two typical specimens, I2205-200 and S304-130, are plotted in Fig. 11.

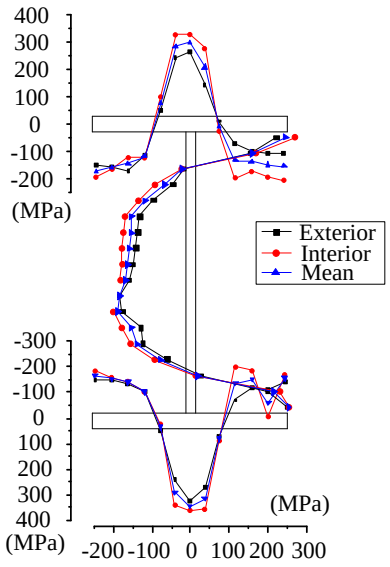

(a) I2205-200

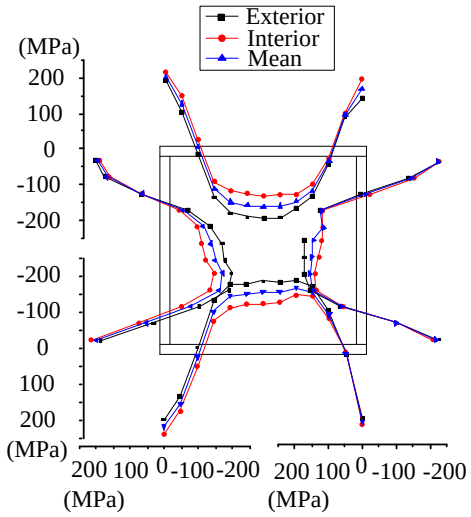

(b) S304-130

Fig. 11 Residual stress distributions in Specimens I2205-200 and S304-130

The variation between the measurements taken on the interior and exterior surfaces of the sections was relatively small. The mean values of these stresses were therefore taken to represent the residual stress state in the sections; this corresponds to the assumption of a uniform strain distribution through the plate thickness. For the I2205-200 specimen, the maximum tensile residual stress was 329 MPa ($0.57\sigma_{0.2}$) in the flange, and the maximum compressive residual stress reached 186 MPa ($0.34\sigma_{0.2}$). For the S304-130 specimen, the peak values of tensile and compressive residual stresses were 227 MPa ($0.73\sigma_{0.2}$) and 171 MPa ($0.61\sigma_{0.2}$), respectively. Simplified residual stress distribution models for stainless steel built-up sections will be devised once further planned residual stress measurements are made.

5 Stub column tests

5.1 Instrumentation and testing procedure

A total of 28 stub column tests were performed. Four symmetrically placed LVDTs (see Fig. 12) were used to determine the end shortening of the stub columns. Strain gauges were attached to the mid-faces of the cross-sections to monitor local buckling of the plates, while corner gauges were used for alignment of the specimens. Fig. 12 shows the detailed instrumentation layout at mid-height of the tested cross-sections. Twelve strain gauges were used for the I-section stub columns, while eight gauges were required for the RHS and SHS stub columns. Grid lines were drawn onto the outer surfaces of the stub column specimens such that any local buckling could be observed distinctly.

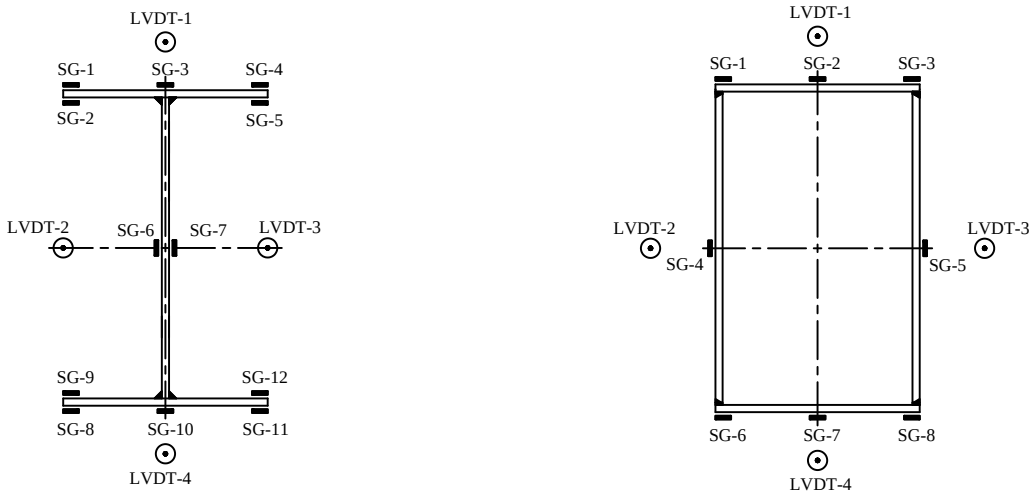

(a) I-section (b) SHS and RHS

Fig. 12 Instrumentation configurations for stub column tests

A spherical upper end bearing plate was adjusted to achieve full contact with the test specimens. After geometrically centreing the stub column specimens, a preloading procedure was carried out to assess the alignment and check the instrumentation system. The spherical end bearing plate was locked into position by four corner bolts to generate fixed end boundary conditions once the alignment work was completed. All the stub column specimens were axially loaded using displacement control by means of a 5000 kN capacity hydraulic testing machine. The loading process of all the test specimens was continued until excessive end shortening and a clear decline in axial load was observed. General views of the test set-up are shown in Fig. 13.

(a) I2205-372 (d) S304-300

Fig. 13 Stub column test set-up

5.2 Test results

Fig. 14 presents all 28 deformed stub column specimens, showing that all the specimens underwent local buckling failure. Some evidence of global buckling may be seen in some of the test specimens, though such behaviour was only observed after the peak load had been obtained. Similarly, five of the six hollow sections of the EN 1.4462 alloy experienced tearing failure of longitudinal welds owing to excessive deformations, but no cracks were evident before the ultimate load was reached.

(a) I-section (b) RHS and SHS

Fig. 14 Deformed shapes of all stub column specimens

The stress-strain curves derived from the stub column tests are plotted in Fig. 15. The stresses were computed by dividing the axial load by the measured cross-sectional area, and the strains were determined from the ratio between the recorded end shortening and the measured stub column length. It may be observed that all the stub columns exhibited rounded stress-strain curves, with the stockier sections in particular revealing significant non-linearity and strain-hardening characteristics. The test results, including the ultimate load $N_{u,Exp}$ and end shortening at ultimate load $\delta_{u,Exp}$ are summarized in Tables 6 and 7.

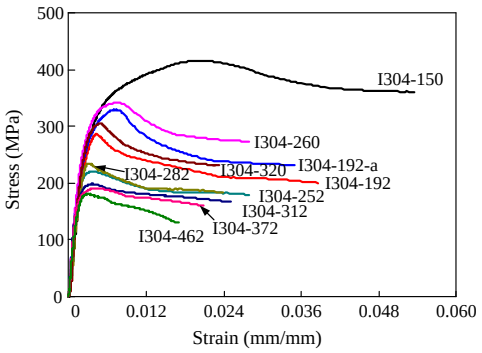

(a) I-section (EN 1.4301)

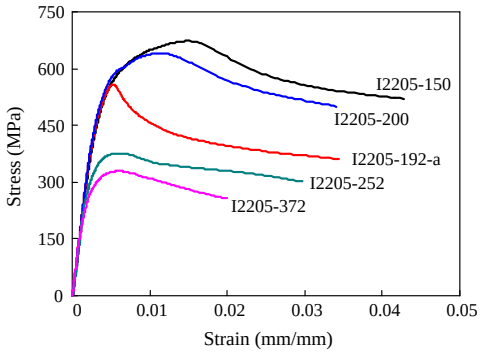

(b) I-section (EN 1.4462)

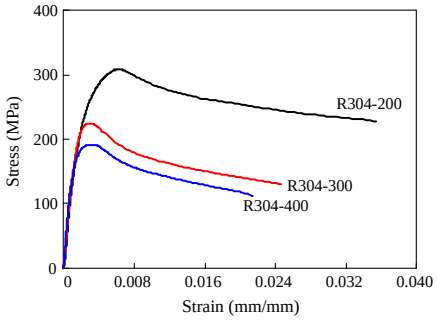

(c) RHS (EN 1.4301)

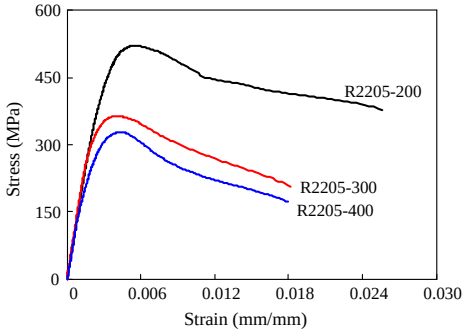

(d) RHS (EN 1.4462)

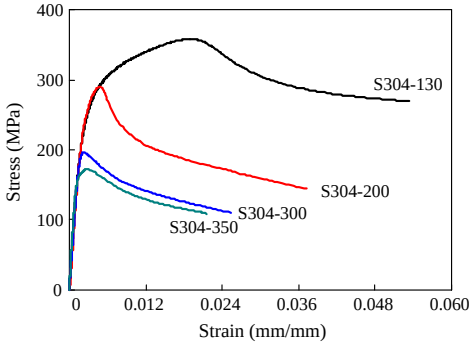

(e) SHS (EN 1.4301)

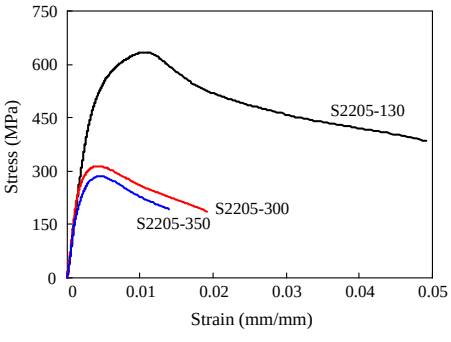

(f) SHS (EN 1.4462)

Fig. 15 Experimental stress-strain curves derived from the stub column tests

In Fig. 16, the ultimate loads achieved by the stub columns $N_{u,Exp}$ normalised by their respective yield loads $A\sigma_{0.2}$ are plotted against the slenderness of the cross-section $\bar{\lambda}_p$, allowing for element interaction. This was defined as $\bar{\lambda}_p = \sqrt{\sigma_{0.2} / \sigma_{cr}}$, where σ_{cr} was obtained from CUFSM [27], using centreline dimensions. Allowance for flat element widths was made by multiplying the resulting slenderness by the maximum value of the ratios of flat to centreline element widths. The graph shows that cross-sections with a slenderness less than about 0.68 reach capacities beyond the yield load as a result of strain hardening, while more slender sections fail prior to yielding due to the occurrence of local buckling.

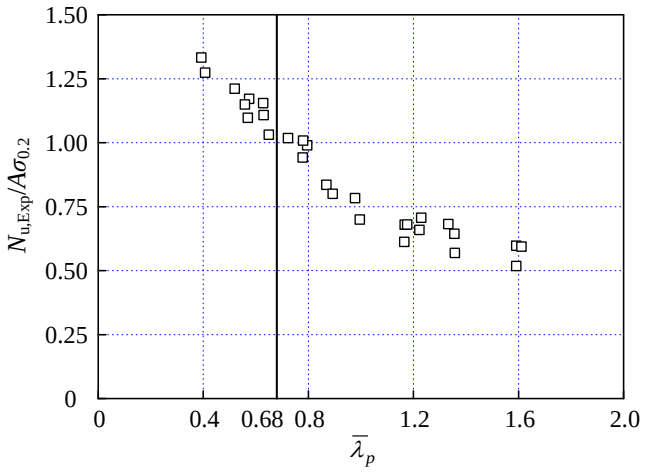

Fig. 16 Test ultimate load versus cross-sectional slenderness

6 Evaluation of EN 1993-1-4 and the CSM

In this section, the obtained stub column test strengths are used to evaluate the current EN 1993-1-4 design provisions and the newly developed CSM. The measured material properties obtained from the compressive coupon tests (LC) were used to calculate the predicted design resistances, in which the 0.2% proof stress $\sigma_{0.2}$ was used as the nominal yield strength f_y. The EN 1993-1-4 design guidelines are based on the cross-section classification concept, in which limiting width-to-thickness ratios for each of the cross-section classes are defined. Once the Class 3 slenderness limit is exceeded, the effective width approach is to calculate an effective cross-sectional area, accounting for the occurrence of local buckling prior to the attainment of the 0.2% proof stress [28]. In EN 1993-1-4, the current Class 3 slenderness limits for internal elements (cold-formed or welded) and welded outstand elements in pure compression are 30.7ε and 11ε, respectively, where ε is a material factor given by Eq. (1):

$$\varepsilon = \sqrt{\frac{235}{f_y}\frac{E_0}{210000}} \tag{1}$$

The local buckling reduction factors for welded Class 4 internal and outstand elements are given by Eqs. (2) and (3), respectively.

$$\rho = \frac{0.772}{\bar{\lambda}_p} - \frac{0.125}{\bar{\lambda}_p^2} \le 1 \quad \text{for internal elements (cold-formed or welded)} \tag{2}$$

$$\rho = \frac{1}{\bar{\lambda}_p} - \frac{0.242}{\bar{\lambda}_p^2} \le 1 \quad \text{for welded outstand elements} \tag{3}$$

in which the element slenderness $\bar{\lambda}_p$ is defined as

$$\bar{\lambda}_p = \sqrt{\frac{f_y}{\sigma_{cr}}} = \frac{\bar{b}/t}{28.4\varepsilon\sqrt{k_\sigma}} \tag{4}$$

where $\overline{b}/t$ is the relevant width-to-thickness ratio and k_σ is the buckling coefficient dependent on the boundary conditions and applied stress conditions.

The EN 1993-1-4 slenderness limits and effective width formulae have also recently been re-evaluated [29]. The test results are therefore also compared against the proposed revised values, which are as follows: the proposed Class 3 slenderness limits for internal and outstand elements (with no distinction made between welded and cold-formed sections) are 37ε and 14ε, respectively. The proposed effective width formulae are given by Eqs. (5) and (6).

$$\rho = \frac{0.772}{\overline{\lambda}_p} - \frac{0.079}{\overline{\lambda}_p^2} \le 1 \qquad \text{for internal elements} \qquad (5)$$

$$\rho = \frac{1}{\overline{\lambda}_p} - \frac{0.188}{\overline{\lambda}_p^2} \le 1 \qquad \text{for outstand elements} \qquad (6)$$

The test capacities are also compared with those predicted by the CSM. The CSM was developed originally in view of the high degree of material non-linearity and strain hardening exhibited by stainless steel alloys. The CSM abandons the concept of section classification, and replaces it with a continuous relationship between cross-sectional slenderness and deformation capacity. Combined with more accurate material modelling, the design resistances can then be determined directly. For plated sections, the normalized deformation capacity $\varepsilon_{csm}/\varepsilon_y$ is given by [30]

$$\frac{\varepsilon_{csm}}{\varepsilon_y} = \frac{0.25}{\overline{\lambda}_p^{3.6}} \text{ but } \frac{\varepsilon_{csm}}{\varepsilon_y} \le \text{minimum}\left(15, \frac{0.10\varepsilon_u}{\varepsilon_y}\right) \qquad \text{for } \overline{\lambda}_p \le 0.68 \qquad (7)$$

where $\varepsilon_y = f_y/E_0$ is the yield strain, $\overline{\lambda}_p$ is the slenderness of the cross-section or its most slender constituent element and ε_u is the strain at the ultimate tensile stress f_u, taken as $\varepsilon_u = 1 - f_y/f_u$ but not more than the elongation at fracture. Note that the CSM does not apply to slender sections, where $\overline{\lambda}_p > 0.68$. For slender sections, reference should be made to existing effective width or direct strength methods.

The stress σ_{csm} corresponding to ε_{csm} may be obtained from

$$f_{csm} = f_y + E_{sh}\varepsilon_y\left(\frac{\varepsilon_{csm}}{\varepsilon_y} - 1\right) \qquad (8)$$

in which the strain hardening modulus E_{sh} can be determined from [30] as:

$$E_{sh} = \frac{f_u - f_y}{0.16\varepsilon_u - (\varepsilon_y + 0.002)} \qquad (9)$$

The measured material and geometric properties were used in the evaluation process. The design resistances of the tested stub columns predicted by the EN 1993-1-4 provisions, including use of the revised slenderness limits and effective width formulae, and the CSM based on cross-section slenderness were compared with the test results, as detailed in Tables 6 and 7. It should be noted that all the partial safety factors were set equal to unity in the comparison.

Table 6 Comparison of stub column test strengths with predicted values from EN 1993-1-4, EN 1993-1-4 with revised slenderness limits and effective width formulae, and the CSM for I-section specimens

Specimen	$N_{u,Exp}$ (kN)	$\delta_{u,Exp}$ (mm)	EN 1993-1-4			Revised EN 1993-1-4			CSM		
			Web class	Flange class	$N_{c,Rd}/N_{u,Exp}$	Web class	Flange class	$N_{c,Rd}/N_{u,Exp}$	$\bar{\lambda}_p$	$\varepsilon_{csm}/\varepsilon_y$	$N_{csm,Rd}/N_{u,Exp}$
I304-150	1568.3	8.8	1	1	0.75	1	1	0.75	0.39	7.2	0.85
I304-192	949.4	2.5	4	4	0.84	2	4	0.91	0.72	-	-
I304-192-a	859.8	4.2	4	3	0.83	2	3	0.85	0.57	1.8	0.87
I304-252	968.8	2.8	4	4	0.89	4	4	0.95	0.98	-	-
I304-260	1622.8	5.8	4	1	0.85	4	1	0.87	0.63	1.3	0.91
I304-282	905.5	2.5	4	4	0.92	4	4	0.99	0.87	-	-
I304-312	1088.7	3.4	4	4	0.82	4	4	0.87	1.23	-	-
I304-320	1804.4	4.4	4	4	0.90	4	3	0.93	0.80	-	-
I304-372	978.5	4.8	4	4	0.90	4	4	0.95	1.17	-	-
I304-462	893.8	3.9	4	4	0.96	4	4	1.02	1.36	-	-
I2205-150	2549.9	6.8	4	3	0.82	1	3	0.83	0.52	2.6	0.86
I2205-192-a	1447.7	3.2	4	4	0.82	4	4	0.90	0.78	-	-
I2205-200	2298.6	7.1	4	1	0.81	4	1	0.82	0.63	1.3	0.87
I2205-252	1653.2	4.5	4	4	0.80	4	4	0.84	1.33	-	-
I2205-372	1686.3	6.4	4	4	0.80	4	4	0.83	1.59	-	-
Mean	-	-	-	-	**0.85**	-	-	**0.89**	-	-	**0.88**
COV	-	-	-	-	**0.05**	-	-	**0.07**	-	-	**0.02**

It can be seen that both the current EN 1993-1-4 and that with the revised slenderness limits and effective width formulae provide generally conservative predictions. According to the EN 1993-1-4 provisions, the mean value of $N_{c,Rd}$/Nu,Exp ratios for I-section specimens is 0.85 with the corresponding coefficient of variation (COV) of 0.05, and the corresponding mean ratio for RHS and SHS specimens is 0.88 with the same COV. The revision of the EN 1993-1-4 slenderness limits and effective width formulae results in an average increase in resistance of about 5%. The CSM comparisons, which have only been made for the non-slender cross-sections (i.e. $\bar{\lambda}_p \le 0.68$), the mean Ncsm,Rd/Nu,Exp predictions and COV are 0.88 and 0.02 for the I-sections and 0.92 and 0.03 for the SHS and RHS. This represents an 8% average improvement in capacity predictions over EN 1993-1-4 for the non-slender sections, and a reduction in scatter. As noted previously, for cross-sections where $\bar{\lambda}_p$ exceeds 0.68, the effective width predictions would be retained.

Table 7 Comparison of stub column test strengths with predicted values from EN 1993-1-4, EN 1993-1-4 with revised slenderness limits and effective width formulae, and the CSM for RHS and SHS specimens

Specimen	$N_{u,Exp}$ (kN)	$\delta_{u,Exp}$ (mm)	EN 1993-1-4			Revised EN 1993-1-4			CSM		
			Web class	Flange class	$N_{c,Rd}/N_{u,Exp}$	Web class	Flange class	$N_{c,Rd}/N_{u,Exp}$	$\bar{\lambda}_p$	$\varepsilon_{csm}/\varepsilon_y$	$N_{csm,Rd}/N_{u,Exp}$
R304-200	1068.6	3.8	4	1	0.85	3	1	0.91	0.57	1.9	0.93
R304-300	1317.1	2.5	4	4	0.94	4	3	1.03	0.89	-	-
R304-400	1351.7	3.3	4	4	0.94	4	3	1.02	1.18	-	-
S304-130	1066.4	7.3	1	1	0.79	1	1	0.79	0.41	6.3	0.89
S304-200	1354.2	2.9	4	4	0.87	3	3	0.97	0.65	1.2	0.97
S304-300	1393.2	2.0	4	4	0.93	4	4	0.99	1.00	-	-
S304-350	1423.9	2.8	4	4	0.93	4	4	0.99	1.17	-	-
R2205-200	1802.5	3.2	4	1	0.86	4	1	0.90	0.78	-	-
R2205-300	2140.4	3.7	4	4	0.89	4	4	0.95	1.22	-	-
R2205-400	2320.3	5.2	4	4	0.84	4	4	0.88	1.61	-	-
S2205-130	1897.5	4.2	4	4	0.85	1	1	0.87	0.56	2.0	0.90
S2205-300	2221.5	3.9	4	4	0.88	4	4	0.92	1.36	-	-
S2205-350	2363.5	4.6	4	4	0.84	4	4	0.88	1.59	-	-
Mean	-	-	-	-	**0.88**	-	-	**0.93**	-	-	**0.92**
COV	-	-	-	-	**0.05**	-	-	**0.07**	-	-	**0.03**

7 Conclusions

A comprehensive test programme on stainless steel built-up stub columns has been described in this paper. A total of 28 stub columns of the EN 1.4301 and EN 1.4462 alloys, including I-sections, SHS and RHS, were tested in pure axial compression. The material non-linearity, anisotropy and asymmetry in tension and compression were determined by tensile and compressive coupon tests. The initial local geometric imperfections and residual stresses in the sections were measured prior to testing. Evaluation of the current EN 1993-1-4 design guidelines, a revised version with new proposed slenderness limits and effective width formulae, and the CSM was conducted based upon the obtained experimental cross-sectional resistances. The comparisons indicated that the current EN 1993-1-4 provisions provided generally conservative resistance predictions, while the revised EN 1993-1-4 allowed more efficient exploitation of the material strength. The CSM offered higher and more accurate strength predictions continuously for the non-slender test specimens.

Acknowledgement

The financial supports from the Specialized Research Fund for the Doctoral Program of Higher Education (No.20110002130002) and Beijing Natural Science Foundation (No.8112018) are both gratefully acknowledged by the authors. The first author also appreciates the financial support from the State Scholarship Fund for sponsoring studying abroad, Academic Scholarship for Doctoral Candidates awarded by Ministry of Education of the P.R. China, and Ng Teng Fong/Sino Support Fund for Doctoral Candidates.

References

Baddoo NR. Stainless steel in construction: A review of research, applications, challenges and opportunities. Journal of Constructional Steel Research, 2008, 64(11): 1199-1206.

Graham G. Structural uses of stainless steel-building and civil engineering. Journal of Constructional Steel Research, 2008, 64(11): 1194-1198.

Gardner L. The use of stainless steel in structures. Progress in Structural Engineering and Materials, 2005, 7(2): 45-55.

Rasmussen KJR, Hancock GJ. Design of cold-formed stainless steel tubular members. I: Columns. Journal of Structural Engineering, 1993, 119(8): 2349-2367.

Young B, Liu Y. Experimental investigation of cold-formed stainless steel columns. Journal of Structural Engineering, 2002, 129(2): 169-176.

Liu Y, Young B. Buckling of stainless steel square hollow section compression members. Journal of Constructional Steel Research, 2003(59): 165-177.

Young B, Lui WM. Tests of cold-formed high strength stainless steel compression members. Thin-Walled Structures, 2006, 44(2): 224-234.

Gardner L, Nethercot DA. Experiments on stainless steel hollow sections – Part 1: Material and cross-sectional behaviour. Journal of Constructional Steel Research, 2004, 60(9):1291-1318.

Gardner L, Talja A, Baddoo NR. Structural design of high-strength austenitic stainless steel. Thin-Walled Structures, 2006(44): 517-528.

Kuwamura H. Local buckling of thin-walled stainless steel members. Steel Structures, 2003(3): 191-201.

Zhen BF. Theoretical and experimental investigations on cold-formed stainless steel columns and beam-columns. Master Thesis. Nanjing: Southeast University, 2010. [in Chinese]

Dabaon MA, El-Boghdadi MH, Hassanein MF. A comparative experimental study between stiffened and unstiffened stainless steel hollow tubular stub columns. Thin-Walled Structures, 2009(47): 73-81.

Theofanous M, Chan TM, Gardner L. Structural response of stainless steel oval hollow section compression members. Engineering Structures, 2009(31): 922-934.

Shen XM. Theoretical and experimental investigations on cold-formed stainless steel beams and compressive plates. Master Thesis. Nanjing: Southeast University, 2010. [in Chinese]

Saliba N, Gardner L. Cross-section stability of lean duplex stainless steel welded I-sections. Journal of Constructional Steel Research, 2013(80): 1-14.

Gardner L. The continuous strength method. Structures & Buildings, 2008, 161(SB3): 127-133.

Gardner L, Ashraf M. Structural design for non-linear metallic materials. Engineering Structures, 2006(28): 926-934.

ASTM A959. Standard guide for specifying harmonized standard grade compositions for wrought stainless steels. West Conshohocken, PA: ASTM International, 2011.

GB/T 228-2002. Metallic materials – Tensile testing at ambient temperature. Beijing: Standards Press of China, 2002. [in Chinese]

GB/T 7314-2005. Metallic materials – Compression testing at ambient temperature. Beijing: Standards Press of China, 2005. [in Chinese]

ASTM E8. Standard Test Methods for tension testing of metallic materials. West Conshohocken, PA: ASTM International, 2008.

ASTM E9. Standard Test methods of compression testing of metallic materials at room temperature. West Conshohocken, PA: ASTM International, 2009.

GB/T 983-1995. Stainless steel covered electrodes. Beijing: Standards Press of China, 1995. [in Chinese]

Ziemian RD. Guide to stability design criteria for metal structures. 6th ed. New York: John Wiley & Sons, Inc., 2010.

Young B, Lui WM. Behavior of cold-formed high strength stainless steel sections. Journal of Structural Engineering, 2005, 131(11): 1738-1745.

Tebedge N, Alpsten G, Tall L. Residual-stress measurement by the sectioning method. Experimental Mechanics, 1973; 13(2): 88-96.

Li Z, Schafer BW. Buckling analysis of cold-formed steel members with general boundary conditions using CUFSM: conventional and constrained finite strip methods. Proceedings of the 20th Intl. Spec. Conf. on Cold-Formed Steel Structures, St. Louis, MO. November, 2010.

EN 1993-1-4. Eurocode 3: Design of steel structures – Part 1.4: General rules–Supplementary rules for stainless steels. CEN. 2006.

Gardner L, Theofanous M. Discrete and continuous treatment of local buckling in stainless steel elements. Journal of Constructional Steel Research, 2008(64): 1207-1216.

Afshan S, Gardner L. The continuous strength method for structural stainless steel design. Thin-Walled Structures, Special Issue for Experts Seminar, 2012. [submitted]